International Journal of Metal and Steel Research Technology
Vol. 1, No. 1, July 2013, PP: 01- 11
Available online at http://acascipub.com/Journals.php

Research article

Experimental Determination of the Fatigue Behavior of Austenitic 316L Stainless Steel under Fatigue and Creep-Fatigue Tests at High Temperature

Khairul Azhar Mohammad[a,*], Edi Syams Zainudin[a], Mohd Sapuan Salit[a], Nur Ismarubie Zahari[a], Aidy Ali[b]

[a]Department of Mechanical and Manufacturing Engineering, Universiti Putra Malaysia, 43400 UPM, Serdang Selangor, Malaysia
[b]Department of Mechanical Engineering, National Defence University of Malaysia, Sungai Besi Camp, 57000 Kuala Lumpur, Malaysia

Tel: +60193673954
[*]Corresponding Author: k.amohd@yahoo.com

Abstract

The aim of this work is to characterize and examine the relative importance of the mechanisms of creep-fatigue interaction on the fatigue life of 316L-type austenitic stainless steel at high temperatures. The experiment were performed at constant load amplitude with a stress ratio of 0.1, and the creep fatigue test was imposed by high temperature with 5 minutes hold times at tensile maximum to predict fatigue life in terms of stress versus number of cycles. The Basquin relation was used to verify how accurate the model is in predicting fatigue life. The result shows that the lifetime of prediction curve is slightly lower than the experimental data by 23 percent. The fatigue limit was successfully characterized and found to be 160.69 MPa. Meanwhile, the introduction of a maximum tensile stress hold in cycling reduces the fatigue life compared to continuous cycling, which decreases the number of cycles to failure. The variation of the fracture surface and microstructure pattern of the creep-fatigue specimens were analyzed using scanning electron microscopy (SEM) and optical microscopy techniques.

Keywords: Fatigue life, Hold time, Creep-fatigue, Austenitic 316l stainless steel, Basquin relation

Introduction

Many engineering components in different industries are operated in conditions in which they are subjected to low cycle fatigue at room and otherwise high temperatures. Components of engineering structures that operate at high temperatures, such as jet engine, pressure vessels, nuclear reactors, and steam and gas turbines in oil and gas plants, are subjected to severe thermal effects and suffer alternative loading. There have been enormous research investments toward investigating the safety and performance of oil and gas plant piping.[1] In the oil and gas industry, steel has been widely used for the transportation of oil and gas. It is believed that steel subjected to cyclic loading at high temperatures will result in severe failure of the pipe materials during operation, requiring replacement of the steel. The most widely used type of steel in this industry is 316L stainless steel, which exhibits good creep resistance and fatigue properties that make it a suitable candidate for

structural materials in gas and oil plants. One of the causes of simultaneous fatigue and creep that occurs in the oil and gas industry and other industries, such as power plants and aircraft engines, is their routine maintenance. Steady operation predominantly contributes to experience fatigue, while start-up and shut-down operations with 'hold' or cruise periods contributing to creep.[2] Cylindrical components, such as pressure vessels, pipes, borers, and driving shafts, are commonly used in engineering structures. Due to a wide range of uses, such as for transmission or storage of fluid in pipes and high pressure vessels, these structures must be assessed with different conditions to simulate different materials, temperatures and loading conditions. Therefore, these components can be very sensitive to applications and environments. Sandhya et al.[3] has extensively investigated the creep-fatigue interaction behavior of austenitic stainless steel [4-9], but the creep-fatigue interaction properties of the relatively new Alloy D9 have not been explored.

Life prediction techniques are important for assessing the service damage resulting from high pressure and elevated temperature creep in any industry that is dependent on metal components. These techniques can be based on either fatigue or creep models depending on the dominating failure mode. However, predictions under certain conditions is complex and well-established models are deficient.[10] The investigation and exploration of deformation and failure mechanisms of creep-fatigue interactions are complex and depend on many tests and material parameters, such as heat treatment, load history, stress and strain level, temperature, hold time, frequency, chemical component, and microstructure.[11] Due to popularity of cylindrical components and the extensive usage of this type of geometry, it is crucial to investigate its high temperature crack initiation and growth and crack propagation phenomena. The interaction of creep-fatigue crack growth might occur due to the enhancement of fatigue crack growth caused by weakening of the matrix in grains or embrittlement of grain boundaries and enhancement of creep crack growth in terms of acceleration of precipitation or cavitation by cyclic loading.[12-14] Over the years, many researchers have focused on tolerance design to determine the lifetime of heavy duty pipes that operate under high mechanical pressure and temperature. The fracture surface are examined using SEM and EDX in order to check the crack initiation of steel and its effect on the fatigue and creep-fatigue damage mechanism at high temperatures. The life of a component under creep-fatigue loading is considerably less than if creep or fatigue were to act alone. For safety considerations, the mode of failure of pressure vessels and pipes, which include are crack initiation, crack propagation and fracture, often need to be considered. Meanwhile, pipes subjected to high temperatures will result in a shorter life compared to the sum of creep damage and fatigue damage incurred separately.

Materials

316L stainless steel is examined in this study, and an image and the dimensions of the specimen is shown in Figure 1. The chemical composition of the material is presented in Table 1. Table 2 shows the mechanical properties of a cylindrical structure of 316L stainless steel. The specimen is fabricated to be an hourglass shaped specimen in accordance to ASTM 606 for fatigue test which has threaded ends inside for gripping purposes.

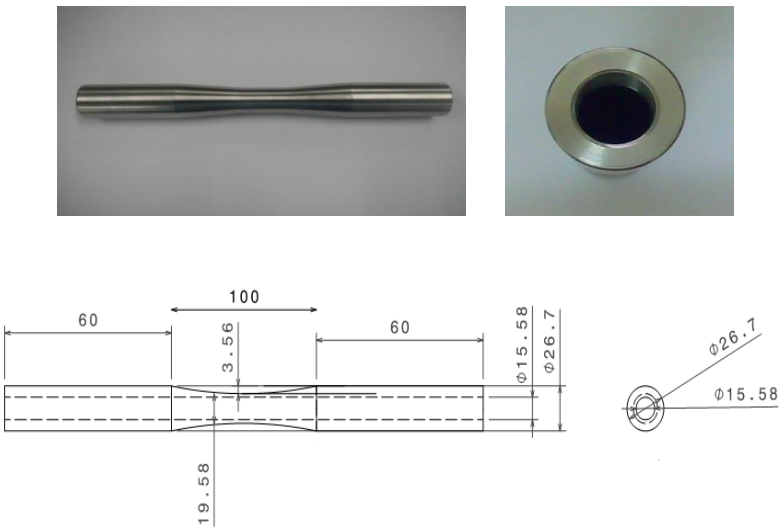

Figure 1: Fatigue specimen and its dimensions in mm

Table 1: Chemical compositions (wt%) of Type 316L stainless steel[15]

Chemical Composition (%)		Austenitic 316L Stainless Steel
Carbon	C	0.020
Nickel	Ni	11.21
Chromium	Cr	17.38
Manganese	Mn	1.860
Phosphorus	P	0.027
Sulphur	S	0.0054
Silicon	Si	0.510
Molybdenum	Mo	2.360
Nitrogen	N	0.038

Table 2: Mechanical Properties of Type 316L Stainless Steel

Mechanical Properties	Type 316L stainless steel
Yield Point, MPa	332
Tensile strength, MPa	673
Modulus of Elasticity, GPa	165
Strength at break, MPa	586
Elongation at break, mm	35.5

Experiment

Fatigue Test

In this study, 316L stainless steel was used to mimic a scenario of oil and gas plant piping in order to determine good safety and reliability parameters. Fatigue tests were conducted at the Strength of Material Lab at Tenaga Nasional Berhad Research (TNBR) in Bangi. The fatigue specimens were tested in a tension-tension fatigue test using a Fast Track Hydraulic Universal Testing Machine Instron 8802 with 250 kN load capacity. All of the specimens used for fatigue testing were monitored to determine the maximum stress and cycle to fail data. Each specimen was attached to the jig at the actuator of the machine. All fatigue tests for the specimens were performed at constant load amplitude, a constant frequency of 5 Hz and a stress ratio of R = 0.1 with a sinusoidal load pattern. The resulting fatigue data, which includes the final data (raw data) was recorded by an Instron 8802 model fatigue system.

Creep Test

Creep tests have been conducted using Zwick/Roell 030 machine at National Universiti of Malaysia. An initial stress of 267 MPa and the high temperature of 565°C is applied and followed according to the ASTM E139-00 standard procedure for conducting creep test of metallic materials using constant load creep tests frames. The specimen elongation was measured using a rod in tube extensometer where ceramic extension arms were attached to the gage length area of the specimen. The axial creep strain was recorded with the help of an arm ceramics touched to the gage length specimen. The furnace of creep machine has the ceramic inside which has maximum temperature rating of 1200^{o}C. Temperature for creep tests was maintained with three zone resistance furnace which was capable of maintaining the temperatures within ±2°C of the test temperature using three thermocouples, whereas all at for each zone furnace. The experiment was taken a 168 hours test as the longest practical test that could be performed considering the number of specimen to be tested, availability of machine and time constraint.

Creep-Fatigue Test

The creep-fatigue tests were carried out similarly to the low-cycle fatigue test, except for the addition of a dwell period at high temperature. For tests with tensile dwell periods, the specimen was held at peak tensile stress for a

period, t_h, with a holding time of 5 minutes at 565°C. The tests were implemented on a closed-loop, servo-controlled, electrohydraulic machine equipped with a resistance type advanced high temperature and environmental system. The temperature of the furnace was controlled by an electronic controller with a type K thermocouple. All the specimens were subjected to repetitive loads to impose a limit on the fatigue life of 10^7 cycles, due to the cost and time constraint of the experiment and specimens. The final results for both of the tests were plotted in graph to show stress versus life data.

Scanning Electron Microscope and microscopic analysis

The microstructures of the material and fracture surface analysis were conducted on both an optical microscope (Leica MS5-M1 150 High Intensity Illuminator) and scanning electron microscope (SEM - Hitachi S-3400N). Fractured surfaces on failed specimens were examined by SEM operating at 15 kV to establish the micromechanics of material failure, identify the initiation site and determine the crack propagation mode. In order to analyze samples using SEM, the analysis was conducted in accordance with ASTM 340-00. For morphological analysis, fracture surfaces were cross-sectioned into proper sizes, which were mechanically polished using a Digital Polisher Machine in order to analyze the microstructure.

Results and Discussion

Validation of the experimental data with a fatigue life model

The results are plotted in the S-N curve shown in Figure 2. From previous research, it should be noted that 316L stainless steel undergoes hardening under cyclic loading.[16] The figures show no failures beyond 9 x 10^3 cycles after the tests were terminated at 9 x 10^7 cycles. Figure 2 shows that the fatigue life for the experimental and model results have a similar variation trend at the same cycles with different stresses. At higher stress, the model fatigue predicted a shorter maximum stress compared to the experimental result. In order to access to validity and utility of a particular model, the experimental data was compared with the Basquin model. In pure fatigue loading, the Basquin analysis predicted a shorter maximum stress, as depicted in the figure, compared to the experimental data. The predicted curve is slightly lower than the experimental data and is 23 percent different.

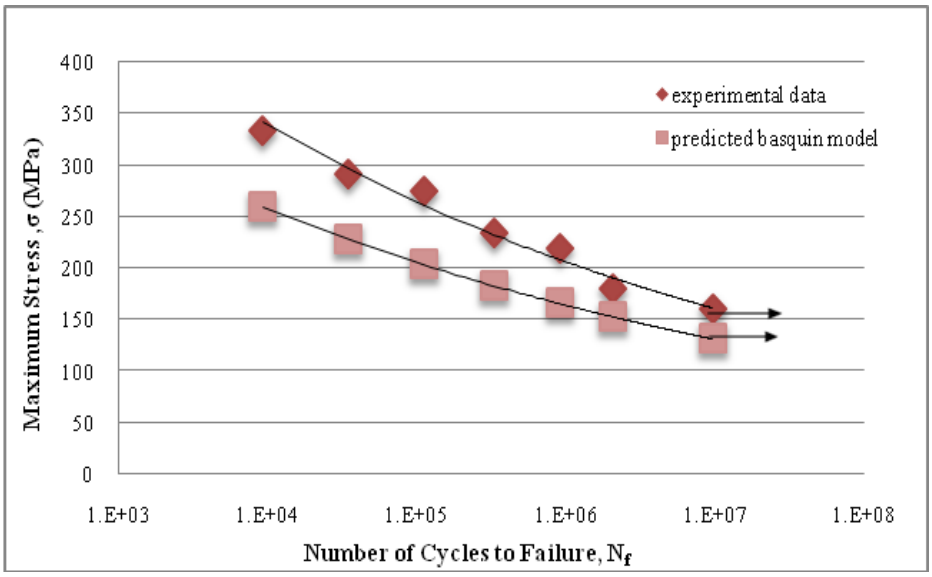

Figure 2: Comparison σ - N of experimental data with predicted fatigue lives for type 316L stainless steel at room temperature

As shown in Figure 2, in the region between 10^6 to 10^7 cycles, the difference in the fatigue limit of steel between the experimental data and Basquin relation is approximately 28 MPa. The Basquin relation is a typical S-N curve, and its expression is developed from log–log S-N graphs and is the most widely used equation. This equation is usable in the stress-based approach to model fatigue analysis and design. The maximum tensile stress for a Basquin relation is given by

$$\sigma_{\max} = \sigma_a = \sigma_f^{'}(2N_f)^b \quad (1)$$

where

$\sigma_f^{'} = 586$ MPa for fatigue strength coefficient (for most metals = σ_f, the true fracture strength), b=-0.142[17] and $2N_f$ is the number of fully reversed cycles to failure. Fatigue tests were conducted using various stress ranges. The fatigue life was calculated by using the Basquin model which is similar to experimental data for the variation trend of the fatigue life curve of austenitic 316L stainless steel.

Maeng et al. and Kim et al.[15,16] noted that the susceptibility of lower fatigue strength could be induced/caused by process fabrication, stress level and shape and has been characterized in this study. The fatigue limit was experimentally observed in the range of 10^6 to 10^7 cycles at a maximum stress of approximately 335 MPa and 260 MPa for predicted data. Failures were observed from 9,000 cycles, and the imposed limit of testing was set to end at 9 x 10^7 cycles, due to time and cost limitations. According to other researchers, the lower fatigue limit in predicted results compared with experimental results is due to the inherent micro-structural in homogeneities in the material, differences in the surface and test conditions of each specimen, and other factors.[18] Table 3 shows the fatigue life obtained in terms of the number of cycles to failure.

Table 3: The number of cycles to failure

Load Ratio (R)	Max Applied Stress (MPa) Experimental	Life (Cycles) Experimental N_f	Max Applied Stress (MPa) Predicted Basquin Analysis	Mean Stress (MPa)	Stress Amplitude (MPa)
0.1	334.00	9,256	259.46	36.78	30.09
	290.93	34,679	228.26	32.69	26.75
	275.20	110,956	203.91	28.61	23.40
	234.33	329,876	183.46	24.52	20.06
	220.15	900,893	166.42	20.43	16.72
	180.11	2,067,895	153.53	16.35	13.37
	160.69	9,664,567	132.21	12.26	10.03

From the results in Table 3, a stress versus fatigue life is plotted to show the significant difference of fatigue life at high stress compared to lower stress. For the predicted analysis, the fatigue life exhibits approximately a 19-25 percent (28-75 MPa) reduction in life. In order to validate the experimental results, previously published experimental data were used for comparison. For instance, the results were compared with the results found by Kim et al.[16] and Maeng et al.[15] It is interesting to note that the σ_{FL} from Kim = 100 MPa and the σ_{FL} from Maeng is = 73.5 MPa. The major difference in these observed σ_{FL} is believed to be due to the different grain sizes and shapes of the specimens as a result of machining into cylindrical or plate forms. According to Kim et al.,[16] experimental stresses increased as compared with the predicted results with the addition of nitrogen in 316L stainless steel due to the strong interaction between nitrogen and chromium. However, these effects were not taken into account in the Basquin analysis. Predicted data of maximum applied stress was determined by Basquin model where 586 MPa as $\sigma_f^{'}$ is the fatigue strength coefficient, *b*=-0.142 is Basquin exponent,[17] and N_f is number of cycle to failure as shown in Table 3. In order to conduct the fatigue testing, the mean stress and stress amplitude are required as the input data in machine operation set up to test the specimen from higher load to lower load.

International Journal of Metal and Steel Research Technology
Vol. 1, No. 1, July 2013, PP: 01- 11
Available online at http://acascipub.com/Journals.php

Creep Deformation

Figure 3 shows that the strain versus time curves where the lifetime was extended by an increased duration of the steady state creep region only. The creep behavior of material under 15 kN, 18 kN, 25 kN and 29 kN are shown in Figure 3. As can be seen from the figure, the magnitude of the creep constants reflects the dominance of secondary creep in the creep curves, particularly at the higher stress levels. The results of creep test under different load has been compared by increasing in the load of strain versus time whereas has increased that slope under 29 kN followed by 25 kN, 18 kN and 15 kN. It founds that increased strains might due to the applied load on specimen at similar temperature.

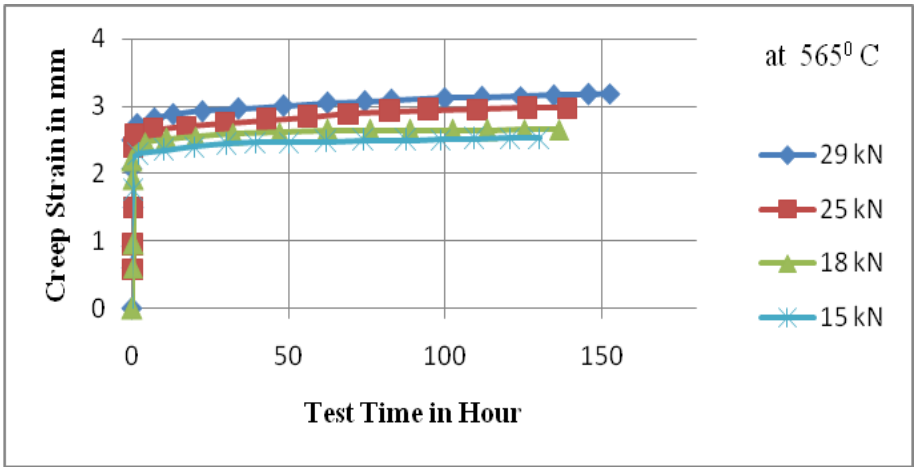

Figure 3: Isochronous $\varepsilon - t$ curve generated for Type 316L stainless steel at 565°C for different loading

Steady-state creep look like to found at beginning of primary stage in tested specimen as shown in the figure, with the primary creep strain contribution to the overall strain being minimal. Besides, as can be seem clearly in Figure 3, lifetime is decreased due to the increase of the strain rate for the creep tests at different applied stress. Based on previous study, initially the creep strain was smooth with increase of deformation. It reached a maximum value after increased load until a further constant was achieved. The maximum creep strain might cause by the increasing in applied stress. Creep deformation is highly dependent on test temperature and stress level. Therefore, we can conclude that the strain rate is increased by rising load. Creep deformation tests were performed on tested specimen condition at 565°C under different stress levels to obtain creep constants for the secondary creep stage using power law (Norton law) relationship to represent the creep deformation behavior.

$$\dot{\varepsilon} = A\sigma_c^n \qquad (2)$$

where,

$\dot{\varepsilon}$ is strain rate, σ is applied stress, A is the stress co-efficient and n is the stress exponent. The data collected from the test have been fitted by power law curves in order to describe the specimen fatigue behavior. The constant A and n of Equation (2) are 1×10^{22} and 6.351 respectively which is obtained from fitted line in power law (Norton law) of experimental data whereas to predict the value of strain rate, $\dot{\varepsilon}$. The value of stress exponent depends on their creep deformation which subjected to the components. For example, stress exponent is indicative of the rate controlling deformation mechanisms.[19] Figure 4 shows the comparison between experimental data and fitted from the creep model generated for each condition using the constitutive Equation (2). The accuracy of the creep constants can be judged from the quality of this model.

Figure 4 shows that the variation of minimum creep rate with applied stress for type 316L stainless steel at 565°C. The curve of variation creep rate versus applied stress is obeyed with a power law (Norton Law) relationship. Furthermore, the creep ductility is higher at 300 MPa compared with the specimen at the 250 MPa. It indicated that the specimen from higher stress had significantly lowered the resistance to creep deformation.

International Journal of Metal and Steel Research Technology
Vol. 1, No. 1, July 2013, PP: 01- 11
Available online at http://acascipub.com/Journals.php

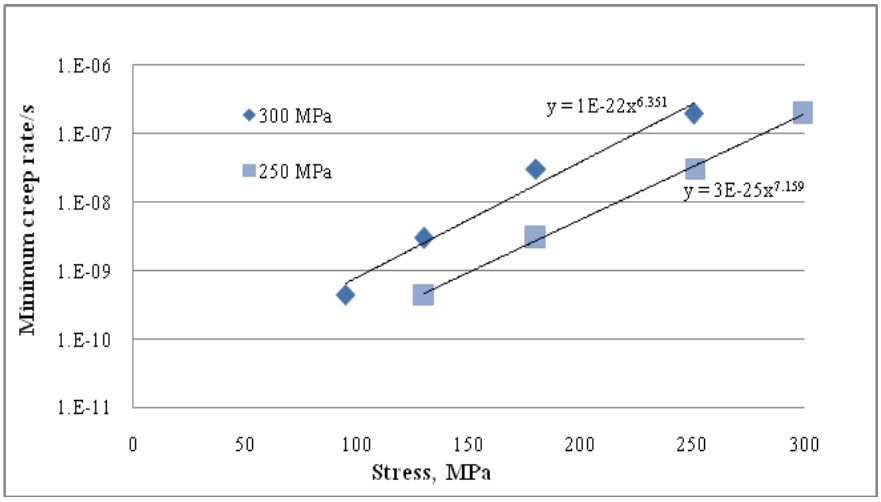

Figure 4: Creep deformation data for Type 316 L stainless steel and fit generated using creep constant

Comparison between Continuous Fatigue and Hold Time Fatigue Tests

In this section, the experimental results of smooth specimens of steel under continuous fatigue and hold-time creep-fatigue tests will be discussed. The results for 316L stainless steel will be discussed for structures operating at high temperature, fatigue and creep damage that accumulates simultaneously based on creep fatigue interaction concurrent with creep-fatigue interaction damage mechanics.

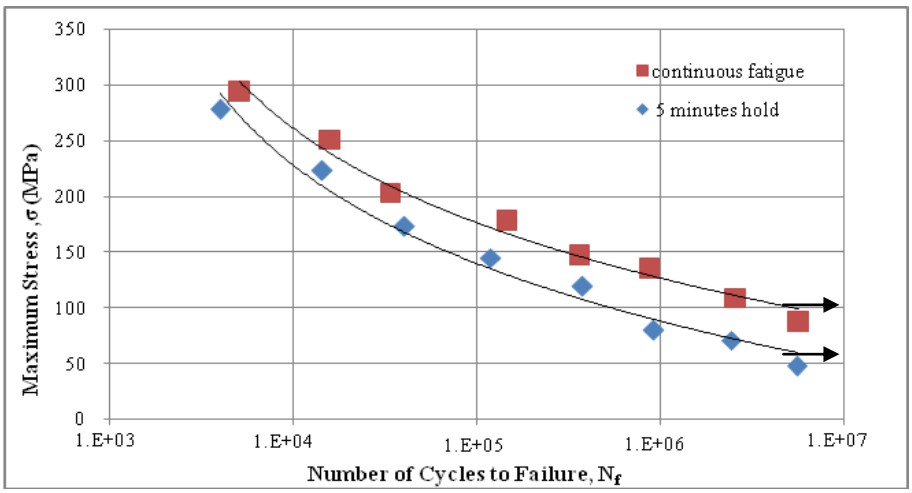

Figure 5: Comparison of continuous fatigue and hold-time fatigue at high temperature

Figure 5 shows the maximum stress plot versus number of cycles to failure for this steel specimen in continuous fatigue and hold times (5 minutes) at elevated temperatures. An introduction of a maximum tensile stress hold (5 minutes) in cycling is presented to identify percentages of creep mechanism occurs in creep fatigue tests in Figure 5. It was observed that the introduction of hold times in tensile periods decreases the number of cycles to failure. Furthermore, the time to failure is higher than during the continuous fatigue test. The fatigue life of this metal decreases considerably with increasing temperature up to 565°C with hold time compared to the continuous fatigue cycling. The fatigue life is shorter with a longer hold period.[20] From continuous to hold times, the change in fatigue life is lower at high temperatures. The fatigue life decreases with an applied tension hold at a temperature of 565°C. The steel material shows an increase in the number of cycles to failure when different loads were applied to the specimen and when a 5-minute hold period is introduced at peak tensile stress. The reduction in life is less when a 225 MPa load is applied on the steel compared to continuous fatigue at 565°C. The application of a tensile hold period in cyclic loading has a marked detrimental effect on the fatigue life of materials.[3]

Previous studies showed that the numerous hold time has been introduced. A 60 minute hold time lengths will lead to the reduction in life cycle fatigue lifetime in high temperature and it will approaching the saturation level. From literature review, the fatigue limits was found as 10^3-10^4 as it is subjected to 10 minutes of hold time to compare with continuous fatigue as 10^2-10^3.[16] According to Conway,[21] beyond a certain hold period duration the relaxed stress was so low and there was a little creep damage occurred for a longer hold time. The absolute value of the maximum tensile stress drops significantly with increasing temperature at a certain stress. The detrimental effects of hold times on 316L steel in air and elevated temperatures may result in a more severe loss of life at high temperatures. The graph shows further reduction in life after a 5-minute tensile hold time, indicating environmental damage and time-independent material, whereby steel is experienced the creep mechanism take precedence over fatigue damage. Creep strain imposed on fatigue results in damage accumulation for 316L stainless steel during hold-time loading compared to continuous fatigue loading. Normally, the crack initiation times for steel are considerably shortened (about 15%), due to higher stress in the process zone where damage occurs.[22] The shorter initiation times for steel may be due to its higher creep exponent and secondary creep rate. The maximum stress and cycles to failure in continuous fatigue steel is higher than that of hold-time fatigue steel. The number of cycles to failure is 2,357,867 for hold-time fatigue steel and 5,978,674 for continuous fatigue steel at 145 MPa. The fatigue for both of continuous and cycling with hold time was 83.7 MPa and 48.9 MPa, respectively. A fatigue life increase of about 5% in creep fatigue steel at continuous cycling was shown as compared to that of creep fatigue with a 5-minute hold time. The trend in variation for 316L stainless steel from the figure suggested that the damage accumulation in steel is overcomed by creep dominated for 5 minutes hold time loading as a minor decrease (10%) approach from pure creep to continuous fatigue loading at a load ratio of 0.1. An intergranular mode of crack propagation at a load ratio of 0.1 is observable as the introduction of short hold times (<5 minutes) was applied.

Microstructural and Chemical Composition Study

There are three stages fracture modes associated with fatigue deformation modes where they were affected by high fatigue sequence loading and propagation of grain boundary cavities within the bulk of the materials.[23] According to Kim et al.,[16] crack initiation in fatigue is dependent on such conditions as stress amplitude, test temperatures, and slip character of the material being tested. The crack nucleates at the surface of the specimen and propagates further into the interior. Meanwhile, crack initiation in FSW 2024-T351 was influenced by stress level, severity of surface irregularities, materials defects such as inclusions, and porosity according to Ali.[24]

Fracture Creep-Fatigue Test Specimen

The specimens were tested at R = 0.1 in pure fatigue loading at 565^{o}C for the creep-fatigue test and showed a transgranular cracking mode, as shown in Figure 6(b). The SEM analysis showed that the crack growth was transgranular and characterized by ductile fatigue striations.[25] Damage within the grains and grain boundaries could be observed for 5-minute hold-time experiments. In this stage, creep damage and void formation was found, whereas they were a characteristic mode of failure. At a load ratio of 0.1, the fatigue test specimen shows ductile fatigue striations, as shown in the figure. Figure 7(b) shows that the SEM fractographs of the 5-minute hold-time test revealed extensive intergranular secondary cracking on grain boundary facets. Striations on the fracture surface were absent. Fracture generally appears to be in mixed mode. It appears that the creep-failure mechanism is the dominant mode of failure for higher hold time tests. The 5-minute hold-time fractograph reveals dimpled rupture with evidence of secondary cracking, and the grain boundary facets are clearly visible. The optical and scanning electron micrograph do not indicate bulk creep cavitation for specified load ratio of 0.1, implying that the deformation is dependent on matrix ductility and consequent tearing when uniaxial creep ductility is exceeded.

The last stage, as shown in Figure 8, is the final mechanism in which separation of the specimen occurs by rapid shear fracture through a heavily cavitated material region. Raj and Ashby[26] noted that the mechanics of creep crack initiation and growth complex are influenced by such parameters as grain size, temperature, strain rate and distribution of second-phase particles at grain boundaries. Austenitic stainless steels are extremely susceptible to intergranular corrosion when they are exposed to temperatures in the range of 425^{o}C to 950^{o}C.[27] The dimpled rupture indicates that more ductility and grain boundary cracking can be observed. According to Raj and Ashby,[26] creep deformation is considerably produced during the hold time where it is plays a role in cavity nucleation and growth and may go through to an intergranular failure mode. Dimples generally result from microvoid coalescence at the grain boundary and are indicative of intergranular fracture.[25] The fatigue striations are separated and absent, while microvoids coalescence at the boundary of the grains, as shown in Figure 8(b).

International Journal of Metal and Steel Research Technology
Vol. 1, No. 1, July 2013, PP: 01- 11
Available online at http://acascipub.com/Journals.php

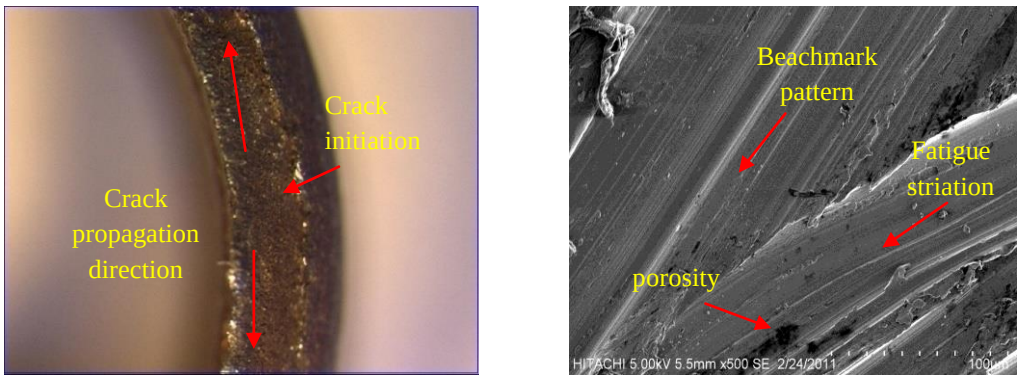

(a) (b)

Figure 6: Optical and SEM observation of the fracture surface after hold tensile fatigue test at 565^{o}C for the primary stage (a) macroscopic surface (b) SEM micrograph

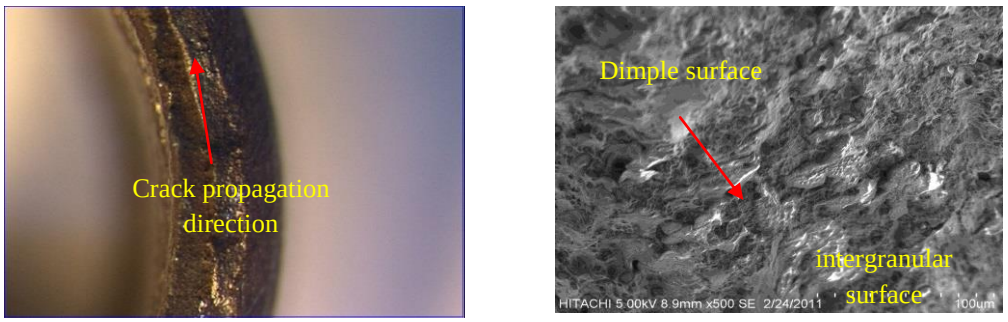

(a) (b)

Figure 7: Optical and SEM observation of the fracture surface after hold tensile fatigue test at 565^{0}C for the second stage (a) macroscopic surface (b) SEM micrograph

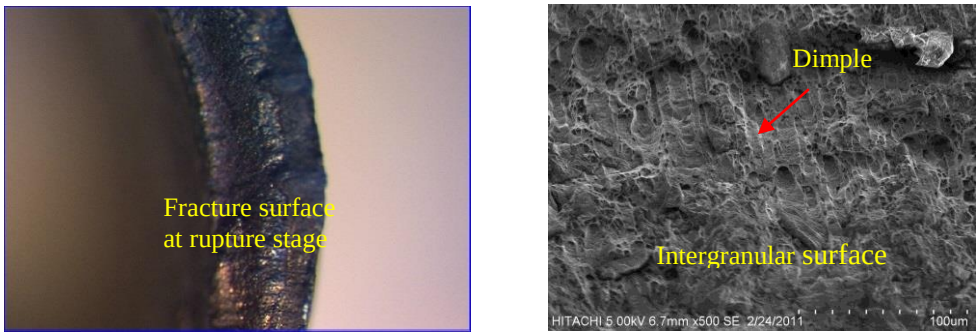

(a) (b)

Figure 8: Optical and SEM observation of the fracture surface after hold tensile fatigue test at 565^{o}C for the third stage (a) macroscopic surface (b) SEM micrograph

Conclusions

1. The fatigue limit of 316L stainless steel is successfully characterized and found to be 87.8 MPa and 39.2 MPa for continuous and 5-minutes hold fatigue tests. Meanwhile, a comparison between both the experimental and predicted data yielded limits of 160.69 MPa and 132.21 MPa, respectively.
2. The fatigue crack growth mechanisms of this material are associated with creep fatigue caused by temperatures, stress, and microstructure. The creep fatigue loading condition is a complex damage mechanism, but it still can be understood at a microstructural level. At low stress, both the continuous and cycling with hold time tests exhibit crack initiation and propagation in a

predominantly transgranular fracture mode. However, this behavior is more apparently in cycling with hold time tests due to creep effects. The anatomy of the cracks tends to shift from transgranular to intergranular as the stress increases.

3. The SEM and EDX experiments showed that the cracks initiate and propagate in mixed mode at the first initiation stage. Both experiments found that intergranular fracture modes dominate the secondary stage at high temperatures. The experiment's results indicate that a transition from the transgranular mode at the early propagation stage to final intergranular fracture is influenced by the grain size at high temperature.

Acknowledgments

The authors would like to thank the University Putra Malaysia under the Research University Grant Scheme (RUGS) (Project No.: 9348000) for its financial in completion the research successfully. We would also like to thank one of the authors, Khairul Azhar bin Mohammad, who made this research possible.

References

[1] Maze, Vanadium sustains the strength of steel at high temperatures for prolonged periods, Vanadium International Technical Committee,
http://www.vanitec.com/pages/en/information/industries/energy.php, (accessed on November 26, 2010)

[2] F. Djavanroodi, Creep fatigue crack growth interaction in nickel base alloys, American Journal of Engineering and Applied Sciences 5 (5) (2008) 454-460.

[3] R. Sandhya, K. R. Bhanu Sankara, S.L. Mannan, Creep-fatigue interaction behavior of a 15cr-15ni, ti modified austenitic stainless steel as a function of ti/c ratio and microstructure, Materials Science and Engineering: A 392(1-2) (2005) 326-334

[4] D.S. Wood, J. Wynn, A.B. Baldwin, P.O. Riordan, Some creep/fatigue properties of type 316 steel at 625oc, Fatigue and Fracture of Engineering Materials and Structures 3 (1) (1980) 39-57.

[5] J. Wareing, Creep-fatigue behaviour of four casts of type 316 stainless steel, Fatigue and Fracture of Engineering Materials and Structures 4 (2) (1981) 131-145.

[6] P.S. Maiya, S. Majumdar, Elevated temperature low cycle fatigue behavior of different heats of type 304 stainless steel, Metallurgical Transactions A 8 (11) (1977) 1651-1660.

[7] C. R. Brinkman, G.E. Korth, Heat-to-heat variations in fatigue and creep-fatigue behavior of aisi type 304 stainless steel at 593oc, Journal of Nuclear Materials 48 (3) (1973) 293-306.

[8] C. R. Brinkman, High temperature time-dependent fatigue behavior of several engineering structural alloys, International Metals Reviews 30 (5) (1985) 235-258.

[9] C. Levaillant, J. Grattier, M. Mottot, A. Pineau, in: Low Cycle Fatigue, ASTM STP 942, eds. H.D. Solomon, G.R. Halfard, L.R. Kaisand, B.N. Leis, America Society for Testing Materials, Creep and creep-fatigue intergranular damage in austenitic stainless steel: discussion of the creep dominated regime, Philadelphia, 1988, pp. 414-437.

[10] S. Kwofie, H.D. Chandler, Fatigue life prediction under conditions where cyclic creep-fatigue interaction occurs, International Journal of Fatigue 29 (12) (2007) 2117-2124.

[11] Z. Fan, C. Xuedong, L. Chen, J. Jiang, Fatigue-creep behavior of 1.25cr0.5mo steel at high temperature and its life prediction, International Journal of Fatigue 29 (6) (2007) 1174-1183.

[12] K.M. Nikbin, G.A. Webster, in : B. Wilshire and D.R.J. Owen (Eds.), Creep-fatigue crack growth in a nickel base superalloy, Pineridge Press, Swansea, 1984, pp 1091-1103.

[13] M.R. Winstone, K.M. Nikbin, G.A. Webster, Modes of failure under creep/fatigue loading of a nickel-base superalloy, Journal of Materials Science 20 (7) (1985) 2471-2476.

[14] V. Dimopulos, K.M. Nikbin, G.A. Webster, Influence of cyclic to mean load ratio on creep/fatigue crack growth, Metallurgical Transactions A 19 (4) (1988) 873-880.

[15] W.Y. Maeng, Y.H. Kang, Creep-fatigue and fatigue crack growth properties of 316ln stainless steel at high temperature, in : Transactions of the 15th International Conference on Structural Mechanics in Reactor Technology (SMiRT-15) Seoul, 1999, pp. 197.

[16] D.W. Kim, J.H. Chang, W.S Ryu, Evaluation of the creep-fatigue damage mechanism of type 316l and type 316ln stainless steel, International Journal of Pressure Vessels and Piping 85 (6) (2008) 378-384.

[17] S.G.S. Ramanband, V.M. Radhakrishnan, On cyclic stress-strain behavior and low cycle fatigue life, Materials & Design 23 (3) (2002) 249-254.

[18] S.M. Beden, S. Abdullah, A.K. Ariffin, N.A. Al-Asady, M.M. Rahman, Fatigue life assessment of different steel-based shell materials under variable amplitude loading, European Journal of Scientific Research 29 (1) (2009) 157-169.

[19] R.A. Claudio, A. Burgess, C. M. Branco, J. Byrne, Failure analysis of scratch damaged shot peened simulated components at high temperature, Engineering Failure Analysis 16 (4) (2008) 1208-1220.

[20] L. Meimei, B.N. Singh, J.F. Stubbins, Room temperature creep–fatigue response of selected copper alloys for high heat flux applications, Journal Nuclear Materials 329–333 Part A (2004) 865-869.

[21] J.B. Conway, J.T. Berling, R.H. Stentz, in : A. E. Carden, A. J. McEvily, Clifford H. Wells, Strain rate and holdtime saturation in low-cycle fatigue: design-parameter plots, Fatigue at Elevated Temperatures, ASTM STP 520, 1973, pp. 637-647.

[22] P.R. Sahm, M.O. Speidel, High-temperature materials in gas turbines, in: Proc. of the Symposium on High-Temperature Materials in Gas Turbines, 1973.

[23] J. Wareing, Creep-fatigue interaction in austenitic stainless steel, Metallurgical and Materials Transactions A 8(5) (1977) 711-721.

[24] A. Ali, M.W. Brown, C.A. Rodopoulos, Modelling of crack coalescence in 2024-t351 al alloy friction stir welded joints, International Journal Fatigue 30 (10-11) (2008) 2030-2043.

[25] R.M. Kain, Evaluation of Crevice Corrosion, Corrosion, 9th edn, ASM Metal Handbook, America Society for Metals, USA, 1987.

[26] R. Raj, M.F Ashby, Intergranular fracture at elevated temperature, Acta Metallurgical Materials 23 (6) (1975) 653-666.

[27] Stainless Steel, Intergranular corrosion of stainless steel tubes, Stainless Steel Tube and Pipe,http://www.stainless-steel-tube.org/Intergranular-Corrosion-of-StainlessSteel Tubes.htm (accessed on 28 April 2011)